16 μm INFRARED HOT ELECTRON TRANSISTOR

S. D. Gunapala, J. K. Liu, J. S. Park, and T. L. Lin
Center for Space Microelectronics Technology
Jet Propulsion Laboratory, California Institute of Technology
Pasadena, CA 91109
U.S.A.

ABSTRACT. We have demonstrated a bound to continuum state $GaAs/Al_xGa_{1-x}As$ infrared hot electron transistor which has a peak response at $\lambda_p = 16.3$ μm. An excellent photo-current transfer ratio of $\alpha_p = 0.12$ and very low dark current transfer ratio of $\alpha_d = 7.2 \times 10^{-5}$ is achieved at a temperature of T = 60 K.

1. INTRODUCTION

Many advanced NASA satellite missions will require long wavelength infrared (IR) instruments out to 19 μm cutoff wavelength. Examples of these instruments are the Atmospheric IR Sounder (AIRS), the Tropospheric Emission Spectrometer (TES), the High Resolution Dynamic Limb Sounder (HIRDLS), and the Stratospheric Wind IR Limb Sounder (SWIRLS) which are being planned for NASA's Earth Observing System (EOS). These space applications have placed stringent requirements on the performance of the IR detectors and arrays including high defectivity, low dark current, uniformity, radiation hardness and lower power dissipation. In addition, the infrared spectrum is rich in information vital to the understanding of composition, structure and the energy balance of molecular clouds and star forming regions of our galaxy. Therefore, NASA has great interest in infrared detectors both inside and outside the atmospheric windows. This paper will present a study and development of a low dark current very long wavelength intersubband IR hot electron transistor (IHET).

There has been a lot of interest recently in the detection of long wavelength (k= 8-12 pm) infrared radiation using multiple quantum wells, due to the fact that these quantum well IR photodetectors [1-13] (QWIPs) and IHETs[8,14-16] can be fabricated using the mature III-V materials growth and processing technologies. This superior materials control results in high uniformity and thus allows fabrication of large staring arrays (k= 8-12 μm) with excellent imaging performance[17-19]. One of the problems associated with the very long wavelength QWIPs is the higher dark current which adversely affects detector

performance. By analyzing the dark current of shallow quantum wells we have realized that the total tunneling current (sequential tunneling + **thermionic** assisted tunneling) is significantly higher than the **thermionic** dark current (Fig. 1). The conduction electrons carrying these two tunneling current components are lower in energy than the photoelectrons Therefore, a 16pm $GaAs/Al_xGa_{1-x}As$ IHET which can effectively filter out sequential tunneling and **thermionic** assisted tunneling currents was fabricated.

2. DARK CURRENT

In this section the dark current of a single quantum well, which has **intersubband** absorption peak at 16 μm will be analyzed. First effective number of electrons [1,20] n(V) which are thermally excited into the continuum transport states, as a function of bias voltage V were calculated, using the following expression.

$$n(V) = \left(\frac{m^*}{\pi\hbar^2 L_p}\right)\int_{E_0}^{\infty} f(E)T(E,V)dE$$
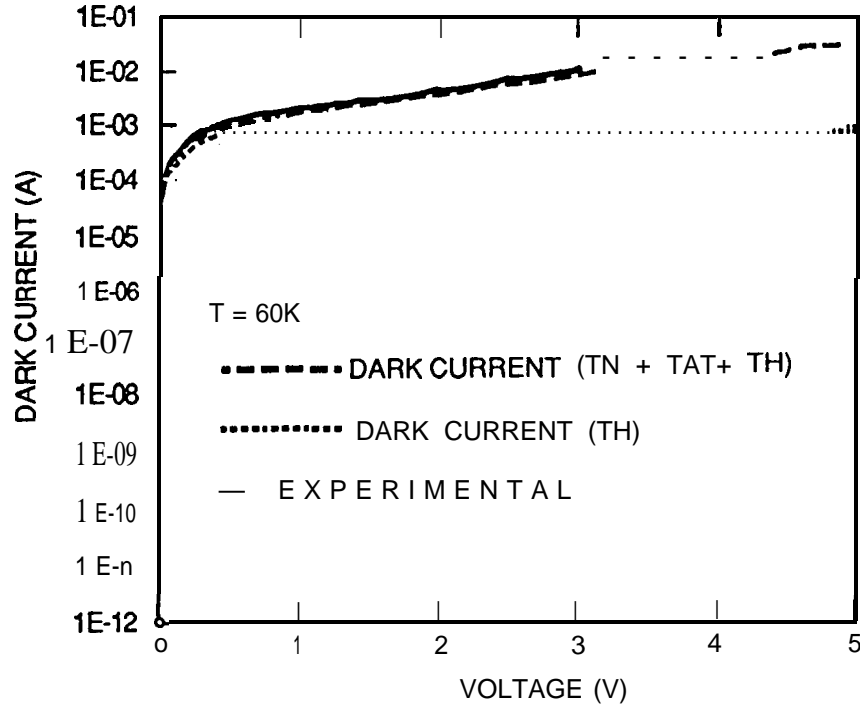
FIG. 1 Theoretical and experimental (solid) dark current-voltage curves at T = 60K. Dotted curve shows the dark current (theoretical) due to **thermionic** emission only. Dashed curve shows the total dark current (**thermionic** + tunneling + **thermionic** assisted) versus bias voltage.

The first factor containing the effective mass m^* represents the average three dimensional density of states. Where L_p is the **superlattice** period, f(E) is the Fermi factor

$f(E) = [1 + \exp(E-E_0-E_F)/KT]^{-1}$, E_0 is the bound state energy, E_F is the two-dimensional Fermi energy, E is the energy of the electron, and $T(E,V)$ is the tunneling current transmission factor. This tunneling transmission factor obtained by applying WKB approximation to a biased quantum well is:

$$T(E) = (4\sqrt{E}\sqrt{(V_0 - E)} / V_0)e^{-2\tau}$$

where $\tau = (2L\sqrt{2m^*} / 3\hbar\Delta V)(V_0 - E)^{\frac{3}{2}}$, V_0 is the barrier height, AV is the bias voltage per superlattice period, and L is the barrier width. The number of electrons, given by n(V), accounts for thermionic emission above the barrier height when $E > V_0$ and thermionic assisted tunneling and tunneling when $E < V_0$. Then the bias-dependent dark current $I_d(V)$ was calculated, using $I_d(V) = eAn(V)v(V)$, where v(V) is the average transport velocity , A is the device area, and e is the electronic charge. The average transport velocity was calculated using $v(V) = \mu F[1 + (\mu F/v_s)^2]^{-1/2}$, where μ is the mobility, F is the electric field, and vs is the saturated drift velocity. In order to obtain T = 60K bias-dependent dark current $\mu = 1200$ cm^2/Vs and $v_s = 5.5 \times 10^6$ cm/s was used. Fig. 1 shows the T= 60K dark current due to thermionic emission, total dark current (thermionic + thermionic assisted tunneling + tunneling), and experimental dark current of a QWIP sample which has wavelength cutoff $\lambda_c = 17.8$ μm. According to the calculations tunneling through the barriers dominate the dark current at temperatures below 30K, at temperatures between 40-60K therrnionic assisted tunneling might become important, and at temperatures above 60K thermionic emission into the continuum transport states dominate the dark current.

3. EXPERIMENT

As shown in Fig.2 the device structure consisted of a multi-quantum well region of 50 periods of 500 Å undoped $Al_{0.11}Ga_{0.89}As$ barrier and 65 Å doped GaAs well. The quantum wells were doped to $n = 5 \times 10^{17}$ cm^{-3}, and sandwiched between a heavily doped ($n = 1 \times 10^{18}$ cm^{-3}) 1 μm GaAs contact layer at the bottom as the emitter contact and a doped ($n = 3 \times 10^{17}$ cm^{-3}) 500 Å GaAs layer on the top as the base contact. On top of the base a 2000 Å undoped $Al_{0.11}Ga_{0.89}As$ layer and a doped ($n = 3 \times 10^{17}$ cm^{-3}) 0.5 μm GaAs layer were grown. The 2000 Å undoped $Al_{0.11}Ga_{0.89}As$ As layer acted as a discriminator between the tunnel-electrons and photo-electrons, and the top 0.5 μm GaAs layer served as the collector. This device structure was grown on a semi-insulating GaAs substrate using molecular beam epitaxy.

The intersubband absorption was measured on a 45" polished multipass waveguide[21] as shown in the inset of Fig. 3. As shown in the Fig. 3 the T = 300K absorption coefficient spectra α_p has a peak infrared absorption coefficient $\alpha_p = 534$ cm-* at $\lambda_p = 17.1$ μm with absorption half heights at 14.2 and 18 μm (i.e., a full width at half maximum of $\Delta\lambda = 3.8$ μm). At low temperature the half width narrows and the peak absorption coefficient increases[22,23] by a factor of 1.3 so that $\alpha_p = 694$ cm-l at T = 60K corresponding to an unpolarized quantum efficiency $\eta = (1 - e^{-2\alpha\ell}) / 2 = 16.5\%$.

To facilitate the application of bias to the quantum well structure, the following processing steps were carried out. First arrays of 200x200 μm^2 square collectors were chemically etched. In the next processing step the 6.25×10^{-4} cm^2 QWIP mesas which overlap with collector mesas were etched. Finally, Au/Ge ohmic contacts were evaporated onto the emitter, base and collector contact layers. The emitter and collector dark currents versus base-collector bias voltage are shown in Fig. 4. This figure also shows the excellent dark current filtration capability of the quantum filter. The dark current transfer ratio
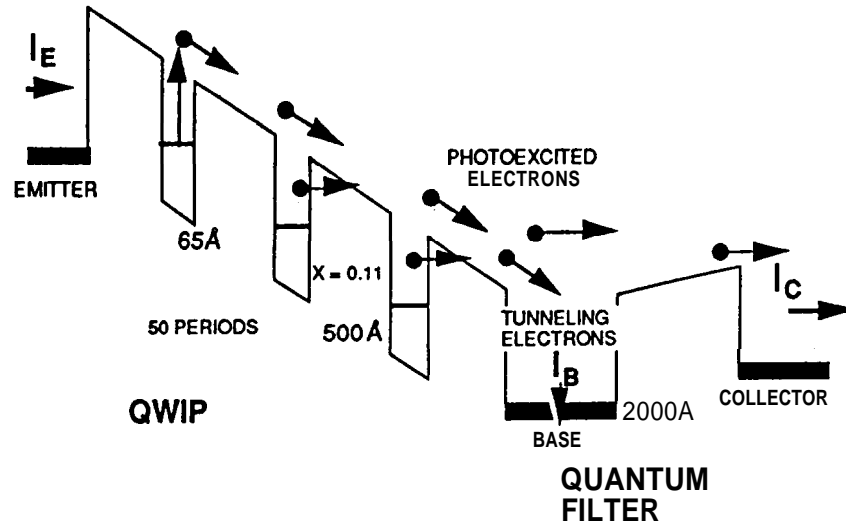
FIG.2 Conduction-band diagram of a infrared hot electron transistor, which utilizes bound to continuum intersubband transition.
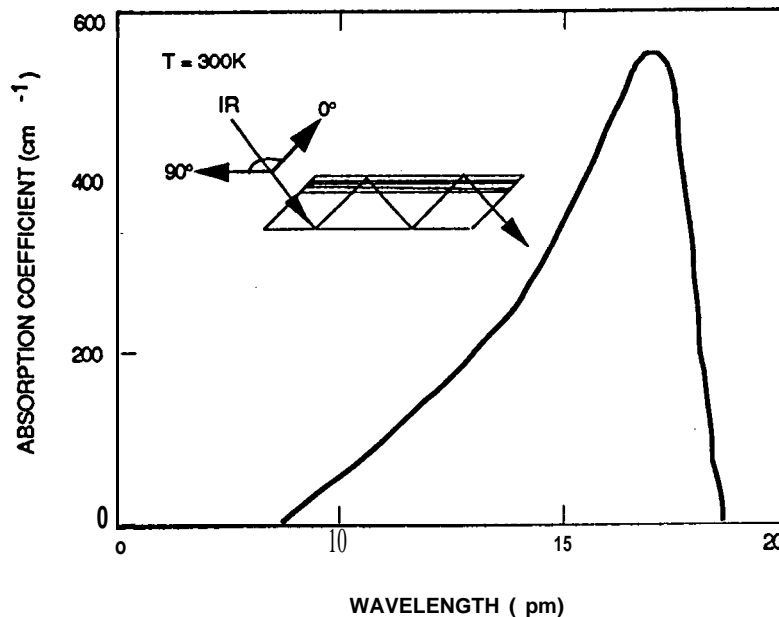
FIG.3 Absorption coefficient spectra et(k) of the long wavelength quantum well infrared detector. This absorption spectra was measured at room temperature using a 45" multipass waveguide geometry as shown in the inset.
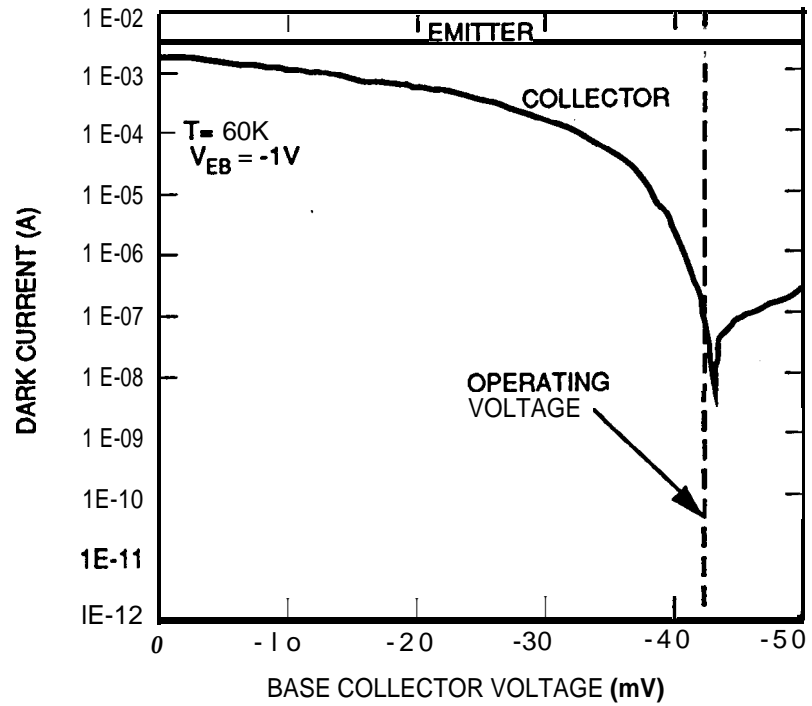
FIG.4 IHET emitter and collector dark currents versus base-collector voltage at T = 60K. Emitter bias was kept at -1V relative to the base potential. This figure also shows the lowerenergydark current filtration capability of the quantum filter.
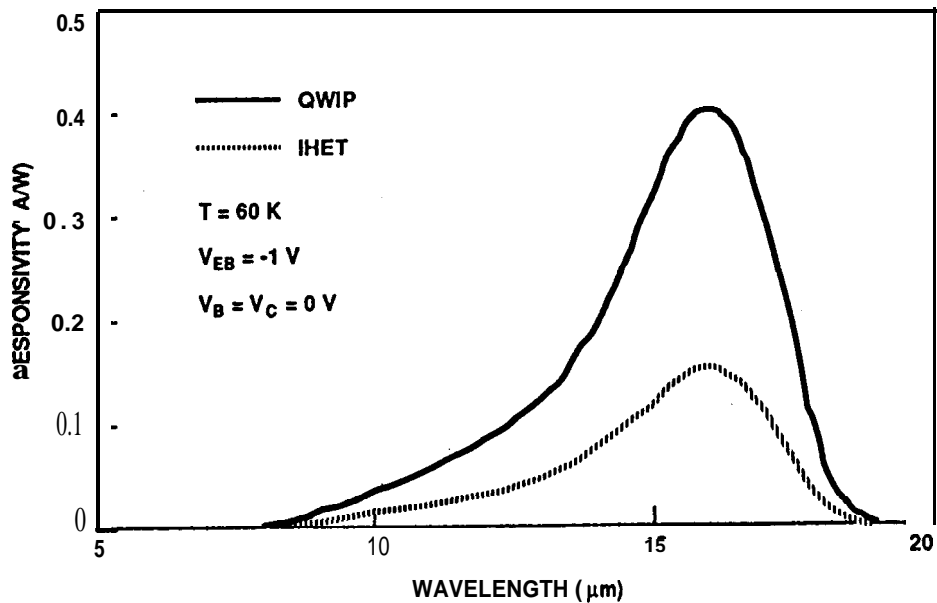
FIG.5 Emitter and collector responsivity spectra at temperature T = 60K. Emitter was kept at -IV bias relative to the base and collector.

$\left(\alpha_d = I_{C(dark)} / I_{E(dark)}\right)$ is **7.2x10-5** at operating base-collector bias voltage V_{CB} = -42 mV (Fig. 7).

These 200x200 μm^2 square detectors were back illuminated through a 45° polished facet as described in detail previously) and responsivity spectra were measured with a tunable source consisting of a lOOOK **blackbody** and a grating monochromator. The emitter and collector responsivity spectrums measured at T = 60K are shown in Fig. 5. These two spectrums are similar in shape and peak at λ_p= 16.3 μm. The values of the cutoff wavelength λ_c and the spectral width (M/~) (full width at half maximum) are 17.3 μm and 20% respectively. The absolute responsivity was measured by two different methods; by comparing the detector photo-response with the photo-response of a calibrated **pyroelectric** detector, and by using a calibrated blackbody source. The peak responsivity Rp of the detector was 400 **mA/W**. Fig. 6 shows the IHET emitter and collector photo currents versus base-collector voltage at T = 60K. The emitter was kept at -1V bias relative to the base potential. Due to the hot electron relaxation in the wide base region, the photo current at collector is smaller relative to the emitter photo current. Photo current transfer ratio $\alpha_p = I_{C(photo)} / I_{E(photo)}$ is 1.2×10^{-1} at V_{CB} = -42 mV (Fig. 7). It is worth noticing that α_d is more than three orders of magnitude smaller than α_p.
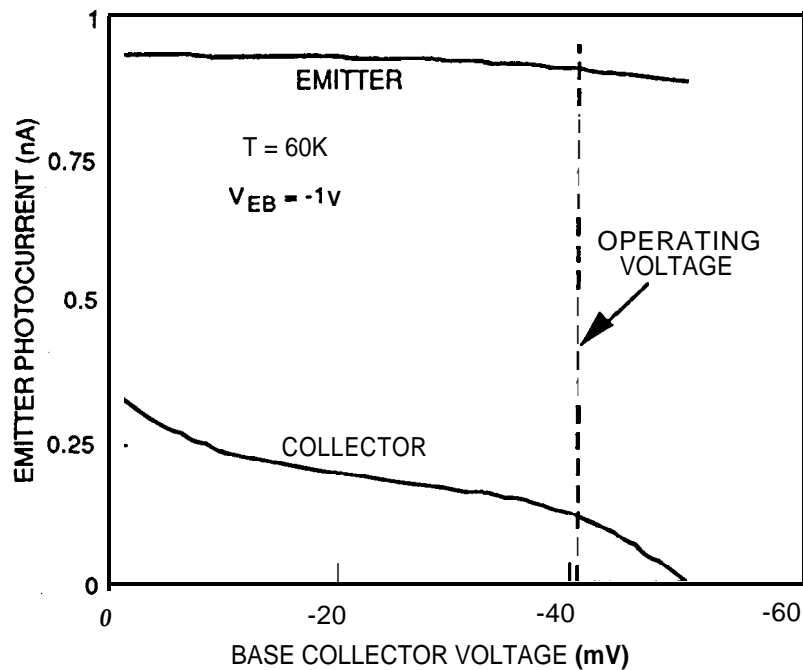
FIG.6 IHET emitter and collector photo currents versus base-collector voltage at T = 60K. Emitter was kept at - 1V bias relative to the base potential.

4. RESULTS

The optical gain g of the detector determined from R = (e/ $h\nu$)ηg is given by g = 0.2. The noise current[24] in was calculated using in = $\sqrt{4eI_dg\Delta f}$, where Af is the bandwidth. The calculated noise current of the detector is in = 17 pA at T = 60K. The peak D^* can now be calculated from D* = R $\sqrt{A\Delta f}/i_n$. The calculated D* between the emitter and the base (QWIP) at V_{EB} = -IV, V_{CB} = -42 mV and T = 60K is 5.8x10^8 cm$\sqrt{Hz}$/W. The defectivity D* at the collector (IHET) is determined) from $D^*(IHET) = (\alpha_p/\sqrt{\alpha_d})$ D*(QWIP). Table 1 shows the QWIP and IHET defectivity D* at temperature T = 60 K for several base-collector bias voltages. As shown in Fig. 8 defectivity D* increases
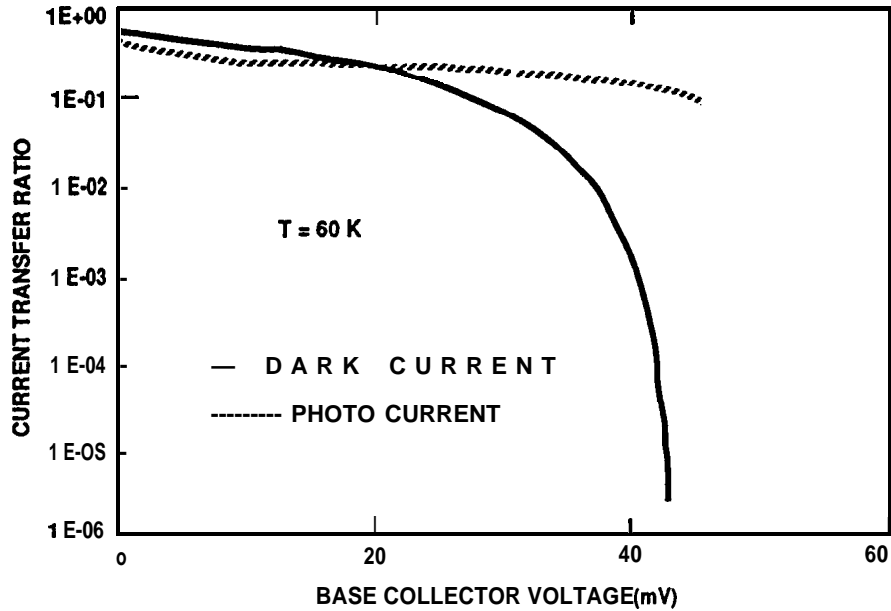
FIG.7 Photo current and dark current transfer ratio of IHET as a function of base-collector bias voltage at temperature T = 60 K.

dramatically with decreasing temperature reaching D*= 1x1012 cm$\sqrt{Hz}$/W at T = 25 K and is even larger at lower temperatures. In contrast, defectivity D^* of HgCdTe detectors are saturated as the temperature is lowered.

5. CONCLUSIONS

In summary, we have demonstrated a very long wavelength (λ_c = 17.3 pm) IHET. This device clearly shows the dark current filtration capability of the energy filter. Therefore, the D* of IHET is much higher than the D* of two terminal multi-quantum well detectors. It is also worth noting that the power dissipation of these detectors are two orders of magnitude smaller than that of HgCdTe detectors. In addition, these detectors show
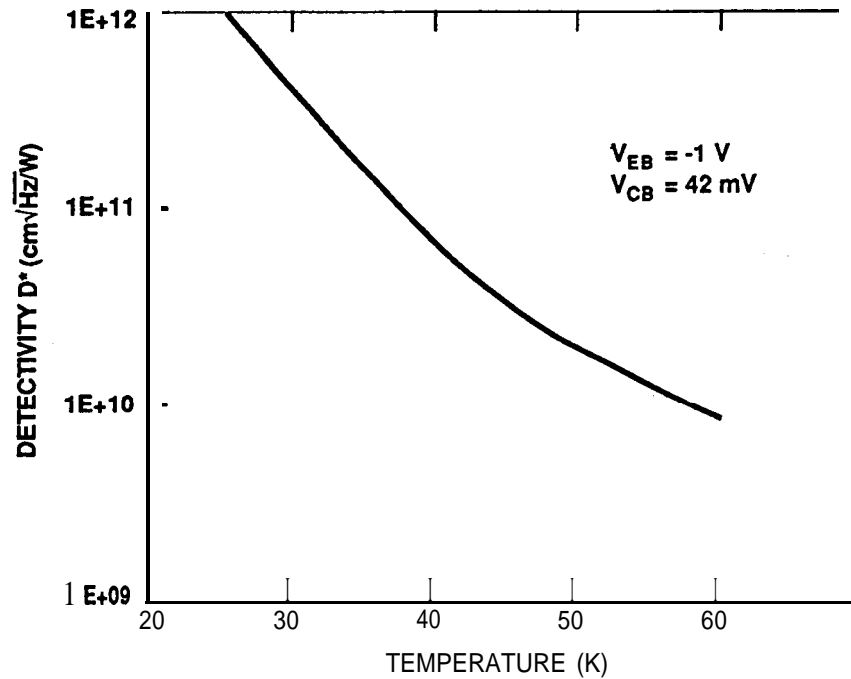
FIG. 8 Peak detectivity D^* for a IHET having a cut-off wavelength of $= 17.3\,\mu m$ as a function of temperature T.

TABLE I. Comparison of QWIP and IHET defectivity D^* at temperature $T = 60$ K for several base-collector bias voltages.

V_{BC} (mV)	$\alpha_p / \sqrt{\alpha_d}$	D^* QWIP (cm√Hz/W)	D^* IHET (cm√Hz/W)
-30	0.72	$6.0X10^8$	$4.3X10^8$
-35	1.17	$5.9X10^8$	$6.9x10^8$
-40	3.98	$5.9X10^8$	$2.3x10^9$
-42	14.14	$5.8x10^8$	$8.2x10^9$

absolutely no change in dark current and responsivity after an exposure of 6.5 Mrad of 1 MeV proton radiations which is equal to 5 years of radiation damage in space. Due to excellent uniformity, radiation hardness, lower powerdissipation and lower I/f noise these GaAs based QWIPs and IHETs are extremely attractive to NASA applications such as EOS missions and IR astronomy.

6. ACKNOWLEDGMENTS

7. REFERENCES

1. B. F. Levine, C. G. Bethea, G. Hasnain, J. Walker, and R. J. Malik, Appl. Phys. Lett. 53.(1988) 296.

2. B. F. Levine, *Proceedings of the NATO Advanced Research Workshop on Intersubband Transitions in Quantum Wells,* Cargese, France Sept. 9-14, 1991 , edited by E. Rosencher, B. Vinter, and B. F. Levine (Plenum, London, 1992).

3. J. Y. Andersson and L. Lundqvist, Appl. Phys. Lett. 59,857 (1991).

4. S. D. Gunapala, B. F. Levine, D. Ritter, R. A. Harem, and M. B. Panish, Appl. Phys. Lett. 58,2024 (1991).

5. S. D. Gunapala, B. F. Levine, D. Ritter, R. A. Harem, and M. B. Panish, Appl. Phys. Lett. 60,636 (1992).

6. B. K. Janousek, M. J. Daugherty, W. L. Bless, M. L. Rosenbluth, M. J. O'Loughlin, H. Kanter, F. J. De Luccia, and L. E. Perry, J. Appl. Phys. 67,7608 (1990).

7. S. R. Andrews and B. A. Miller, J. Appl. Phys. 70,993 (1991).

8. K. K. Choi, M. Dutta, P. G. Newman, M. L. Saunders, and G. L. Iafrate, Appl. Phys. Lett. 57, 1348 (1990).

9. L. S. Yu and S. S. Li, Appl. Phys. Lett. 59, 1332 (1991).

10. A. G. Steele, H. C. Liu, M. Buchanan, and Z. R. Wasilewski, Appl. Phys. Lett. 59, 3625 (1991).

11. S. D. Gunapala, B. F. Levine, L. Pfeiffer, and K. West, J. Appl. Phys. 69, 6517 (1990).

12. M. J. Kane S. Millidge, M. T. Emeny, D. Lee, D. R. P. Guy, and C. R. Whitehouse in Ref. 2.

13. C. S. Wu, C. P. Wen, R. N. Sate, M. Hu, C, W. Tu, J. Zhang, L. D. Flesner, L. Pham, and P. S. Nayer, IEEE Tran. Electron Devices 39,234 (1992).

14. K. K. Choi, M. Dutta, and R. P. Moerkirk, Appl. Phys. Lett. 58, 1533 (1991).

15. K. K. Choi, M. Taysing-Lara, L. Fotiadis, and W. Chang, Appl. Phys. Lett. 59, 1614 (1991).

16. K. K. Choi, L. Fotiadis, M. Taysing-Lara, and W. Chang, Appl. Phys. Lett. 59, 3303 (1991).

17. B. F. Levine, C. G. Bethea, K. G, Glogovsky, J. W. Stayt, and R. E. Labenguth, Semicon. Sci. Technol. 6 (1991) cl 14.

18. M. T. Asom et al., Proceedings of the IRIS Specialty Group on Infrared Materials, Boulder, CO, August 12-16,1991, Vol. I, p. 13.

19. L. J. Kozlowski, G. M. Williams, G. J. Sullivan, C. W. Farley, R. J. Anderson, J. K. Chen, D. T. Cheung, W. E. Tennant, and R. E. DeWames, IEEE Trans. Electron Devices 38, 1124 (1991).

20. B. F. Levine, C. G. Bethea, G. Hasnain, V. O. Shen, E. Pelve, R. R. Abbott, and S. J. Hsieh, Appl. Phys. Lett. 56,851 (1990).

21. B. F. Levine, R. J. Malik, J. Walker, K. K. Choi, C. G. Bethea, D. A. Kleinman, and J. M. Vandenberg, Appl. Phys. Lett. 50,273 (1987).

22. G. Hasnain, B. F. Levine, C, G. Bethea, R. R. Abbott, and, S. J. Hsieh, J. Appl. Phys. 67,4361 (1990).

23. M. O. Manasreh, F. Szmuiowicz, D. W. Fischer, K, R. Evans, and C. E. Stutz, Appl. Phys. Lett. 57, 1790 (1990).

24. B. F. Levine, A. Zussman, S. D. Gunapala, M. T. Asom, J. M. Kuo, and W. S. Hobson, J. Appl. Phys. 72,4429 (1992).

25. S. D. Gunapala, J. S. Park, T. L. Lin, and J. K. Liu (to be published).